

Nuclear obscuration in the high-ionization Seyfert 2 galaxy Tol 0109–383

K. Iwasawa¹, G. Matt², A.C. Fabian¹, S. Bianchi², W.N. Brandt³,
M. Guainazzi⁴, T. Murayama⁵ and Y. Taniguchi^{5,6}

¹*Institute of Astronomy, Madingley Road, Cambridge CB3 0HA*

²*Dipartimento di Fisica, Università degli Studi Roma Tre, Via della Vasca Navale 84, I-00146 Roma, Italy*

³*Department of Astronomy & Astrophysics, The Pennsylvania State University, 525 Davey Lab, University Park, PA16802, USA*

⁴*XMM-Newton SOC, VILSPA, ESA, Apartado 50727, E-28080 Madrid, Spain*

⁵*Astronomical Institute, Tohoku University, Aoba, Sendai 980-8678, Japan*

⁶*Institute for Astronomy, University of Hawaii, 2680 Woodlawn Drive, Honolulu, HI 96822, USA*

ABSTRACT

We report the BeppoSAX detection of a hard X-ray excess in the X-ray spectrum of the classical high-ionization Seyfert 2 galaxy Tol 0109–383. The X-ray emission of this source observed below 7 keV is dominated by reflection from both cold and ionized gas, as seen in the ASCA data. The excess hard X-ray emission is presumably due to the central source absorbed by an optically thick obscuring torus with $N_{\text{H}} \sim 2 \times 10^{24} \text{ cm}^{-2}$. The strong cold X-ray reflection, if it is produced at the inner surface of the torus, is consistent with the picture where much of the inner nucleus of Tol 0109–383 is exposed to direct view, as indicated by optical and infrared properties. However, the X-ray absorption must occur at small radii in order to hide the central X-ray source but leave the optical high-ionization emission line region unobscured. This may also be the case for objects like the Seyfert 1 galaxy Mrk231.

Key words: Galaxies: individual: Tol 0109–383 — Galaxies: Seyfert — X-rays: galaxies

1 INTRODUCTION

It is widely accepted that obscuration is the key for explaining the Seyfert 2 properties in active galaxies (Antonucci 1993). However, the obscuring material in Seyfert 2 nuclei might take various forms or have a complex structure, and its distribution appears to be spread over a wide range of radii (e.g., sub-pc to a few hundred pc), as argued by several authors (e.g., Malkan et al 1998; Taniguchi & Murayama 1998; Matt 2000). Depending on the observational techniques employed, the obscuration inferred of an active nucleus could be different. In particular, optical/near-infrared results often differ from X-ray results (e.g., Goodrich, Veilleux & Hill 1994) as they probe different phenomena taking place at different optical depths. This can, in turn, be used to investigate the structure of obscuration in Seyfert 2 nuclei.

The obscuring matter illuminated by a hidden active nucleus in Seyfert 2 galaxies is an important source of emission over a wide range of wavelengths. While dust reradiation in the far-infrared and some strong optical emission lines, such as [OIII] λ 5007, are considered to be isotropic, any illuminated surface of the obscuring matter could be viewing-angle dependent if it is in the form of a torus

(Heckman 1995). High-ionization emission lines (Pier & Voit 1995; Murayama & Taniguchi 1998), hot ($T_{\text{eff}} \sim 1000$ K) dust emission in the mid-infrared (e.g., Pier & Krolik 1992; Murayama, Mouri & Taniguchi 2000) and X-ray reflection (Ghisellini, Matt & Haardt 1994) are among the observables expected from an illuminated inner surface of an optically-thick torus. These are therefore potential indicators of orientation of the obscuring matter in Seyfert 2 nuclei. Heisler, Lumsden & Bailey (1997) also argued that the detectability of polarized broad-line regions (PBLR) in Seyfert 2 nuclei is related to our viewing angle of the obscuring torus (see also Taniguchi & Anabuki 1999).

X-ray data such as that obtained from BeppoSAX and ASCA have proved to be a powerful probe to heavily obscured active nuclei. Hard X-ray observations available from BeppoSAX penetrate through a large optical depth (e.g., Maiolino et al 1998). X-ray reflection is, as mentioned above, an important diagnostic of the matter directly visible to us and its complex spectral features are better investigated with the reasonable spectral resolution available from ASCA. Here, we present a combined ASCA/BeppoSAX broad band X-ray spectrum of the Seyfert 1.8 nucleus of Tol 0109–383, which exhibits optical properties resembling those

of a Seyfert 1 nucleus in direct view, and yet has a central X-ray source hidden behind an extremely thick absorber, demonstrating segregation of the nuclear obscuration.

2 TOL 0109–383 (=NGC424)

Tol 0109–383 is a southern early-type spiral galaxy at a redshift of 0.0117 (Da Costa et al 1991). This galaxy hosts one of the brightest Seyfert 2 nuclei exhibiting a very high ionization optical spectrum, inferred by the presence of [FeVII] λ 6087, [FeX] λ 6374 and [FeXIV] λ 5303 (Fosbury & Sansom 1985; Durret & Bergeron 1988; Murayama, Taniguchi & Iwasawa 1998). The high ionization region of Tol 0109–383 traced by [FeX] λ 6374 has been found to extend up to 5 arcsec (corresponding to 1.1 kpc for the source distance of 45.3 Mpc^{*}) in radius (Murayama et al 1998), although most (\sim 70 per cent) of the emission is concentrated in the inner 1 arcsec (220 pc) in radius.

An obscured Seyfert 1 nucleus has been suggested for the nuclear activity in Tol 0109–383 (e.g., Boisson & Durret 1986). Broad Balmer emission has been detected in polarized light (Moran et al 2000) as well as in direct light (Boisson & Durret 1986; Murayama et al 1998). Permitted FeII, which is often seen in the spectra of Seyfert 1 galaxies but rarely seen in Seyfert 2 nuclei, has also been detected (Murayama et al 1998). The reddening to the narrow-line regions (NLR) has been estimated to be $A_V = 1.4\text{--}2.0$ (Fosbury & Sansom 1983; Durret & Bergeron 1988; Murayama et al 1998) based on the Balmer decrement, which is comparable to the mean value ($A_V = 1.1$) for Seyfert 2 galaxies (De Robertis & Osterbrock 1986). The Hubble Space Telescope / Wide Field Planetary Camera 2 (HST/WFPC2) image shows clear evidence for a dust lane running across the central part of the galaxy (Malkan et al 1998). This could provide an obscuring screen in front of the nuclear region.

The radio power (e.g., $\log P_{20\text{cm}} \approx 22 \text{ W Hz}^{-1}$, Ulvestad & Wilson 1989), infrared luminosity ($L_{8\text{--}1000\mu\text{m}} = 1.3 \times 10^{44} \text{ erg s}^{-1}$, or $3.4 \times 10^{10} L_{\odot}$, IRAS FSC) and weak UV luminosity ($L_{1450} = 1.9 \times 10^{41} \text{ erg s}^{-1}$, a 100Å-wide band IUE measurement from Mulchaey et al 1994) are typical of Seyfert 2 galaxies. A notable property is the very warm IRAS colour (e.g., $S_{60}/S_{25} = 1.0$), indicating the presence of hot dust. Also, the small size of the radio source, which is only slightly resolved with VLA (at 6 and 20 cm, Ulvestad & Wilson 1989; at 3.6 cm, Threan et al 2000) and ATCA (at 3.5 cm, Morganti et al 1999), is not typical of Seyfert 2 galaxies. Detection of soft X-ray emission with the Einstein Observatory (Green, Anderson & Ward 1992) and ROSAT (Rush et al 1996; Voges et al 1999) has been reported. However, the origin of the soft X-ray emission has not been clear (Murayama et al 1998). Prior to the present paper, Collinge & Brandt (2000) analyzed the ASCA data and concluded that Tol 0109–383 is a Compton-thick source.

* The distance is derived assuming $H_0 = 75 \text{ km s}^{-1} \text{ Mpc}^{-1}$ and a recession velocity with respect to the Galactic Standard of Rest, $V_{\text{GSR}} = 3397 \text{ km s}^{-1}$ (de Vaucouleurs et al 1991)

3 OBSERVATIONS AND DATA REDUCTIONS

Tol 0109–383 was observed with ASCA (Tanaka, Inoue & Holt 1994) on 1997 July 2, and subsequently with BeppoSAX (Boella et al 1997a) on 1999 July 26–28. Details of the observations are summarised in Table 1.

The four detectors on board ASCA, the Solid-state Imaging Spectrometers (SIS; S0 and S1) and the Gas Imaging Spectrometers (GIS; G2 and G3), were operating normally. The Seyfert galaxy was centred at the nominal position on the best-calibrated CCD chips of each SIS detector (S0/C1 and S1/C3). Standard Revision-2 calibration and data reduction technique were employed, using FTOOLS version 4.2 provided by the ASCA Guest Observer Facility at NASA’s Goddard Space Flight Center. The Seyfert galaxy is the brightest source in the detector field of view and there is no other source contaminating the source extraction region in each detector. Background data were taken from a source-free region on the same detector in the same observation. Significant decrease in efficiency of the SIS in the soft X-ray band has been reported in ASCA observations carried out after 1994 (ASCA GOF 1999). The detector responses used here have not been corrected for this effect, but for a faint source like Tol 0109–383, the statistical error overwhelms systematic error in the responses so that the results presented in this paper is not seriously affected.

The BeppoSAX observation provides a dataset from three detectors; the Low Energy Concentrator Spectrometer (LECS, Parmar et al 1997), the Medium Energy Concentrator Spectrometer (MECS, Boella et al 1997b) and the Phoswich Detector System (PDS, Frontera et al 1997). The data from each detector obtained through standard data reduction provided by the SAX Data Centre are used. The background data for the LECS and MECS were taken from the deep blank field observations while the off-source data during the observation are used as the background for the PDS which is a collimated instrument rocking between on and off-source positions.

We quote in this paper values of X-ray flux obtained from the ASCA GIS and BeppoSAX MECS, for which the absolute flux calibration is reliable; indeed the two detectors are in good agreement with each other. The ASCA SIS agrees with the GIS in spectral shape but shows a few per cent smaller normalization than the GIS. The standard relative normalization factor 0.86 is assumed for the PDS. The normalization factor found for the LECS is \sim 0.7, which is within the reasonable range.

4 X-RAY SPECTRUM

4.1 Broad-band X-ray spectrum

Fig. 1 shows the data from all the detectors of BeppoSAX and ASCA, divided by a power-law with a photon-index of $\Gamma = 2$, to demonstrate the broad-band spectral structure of Tol 0109–383. The photon-index $\Gamma = 2.0$, typical of Seyfert nuclei and QSOs, is tentatively used here to demonstrate the energy distribution of the X-ray source (see also similar plots for NGC1068, NGC4945 and NGC6240 in Guainazzi et al 2000 and Vignati et al 1999 for comparison). Because of the complexity of the X-ray spectrum and the present quality of the data, the spectral slope of the central source in this

Table 1. ASCA and BeppoSAX observations of Tol 0109–383. The count rates of two same type of detectors, the SIS (S0/S1) and GIS (G2/G3), are shown.

Satellite	Date	Instrument	Energy range	Count rate ct s ⁻¹	Exposure 10 ³ s
ASCA	1997 July 02	SIS(1CCD/Faint)	0.6–7 keV	$(2.0/1.5) \times 10^{-2}$	47 × 2
		GIS (PH)	0.9–10 keV	$(1.1/1.5) \times 10^{-2}$	31 × 2
BeppoSAX	1999 July 26–28	LECS	0.2–4 keV	2.3×10^{-3}	25
		MECS	2–10 keV	8.9×10^{-3}	64
		PDS	15–100 keV	0.16	32

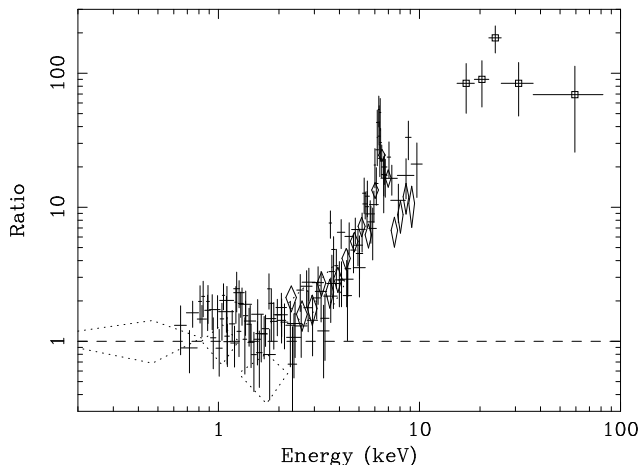


Figure 1. The data from all the detectors of BeppoSAX (diamonds: LECS (dotted) and MECS (solid); and squares: PDS) and ASCA (crosses: SIS and GIS), divided by a power-law of $\Gamma = 2.0$ modified by the Galactic absorption ($N_{\text{H}} = 1.8 \times 10^{20} \text{ cm}^{-2}$). The power-law has been normalized to match the data at 1 keV, where the luminosity is $4 \times 10^{40} \text{ erg s}^{-1} \text{ keV}^{-1}$ for Tol 0109–383.

object cannot be constrained very well, but $\Gamma = 2$ is consistent with the data and we use this power-law slope hereafter (see also Section 4.3). The power-law has been modified by Galactic absorption ($N_{\text{H}} = 1.8 \times 10^{20} \text{ cm}^{-2}$, Dickey & Lockman 1990) and normalized to match the observed flux at 1 keV. The luminosity at 1 keV is about $4 \times 10^{40} \text{ erg s}^{-1} \text{ keV}^{-1}$ for our assumed source distance of 45.3 Mpc.

The continuum spectrum becomes hard above 3 keV: the 3–6 keV continuum has a photon-index of $\Gamma = -0.28_{-0.48}^{+0.44}$, obtained by fitting jointly the ASCA four detectors and the MECS with a power-law. A strong iron K emission line is evident at ~ 6.4 keV (although the BeppoSAX data show a higher line energy, we believe that the line is at 6.4 keV, as found in the ASCA data, which is discussed in detail in Section 4.3). These are consistent with a reflection spectrum from cold matter.

However, cold reflection alone cannot explain the whole range of observed broad-band spectrum. The cold reflection model, e.g., *pexrav*, Magdziarz & Zdziarski (1995), with an illuminating power-law source of $\Gamma = 2$, to match the Fe K band data leaves significant surplus emission above 7 keV observed with the GIS and the PDS. This hard X-ray excess is not prominent in the SIS data due to the sharply declining detector response at those energies. The large hard X-ray excess suggests the presence of a strongly absorbed

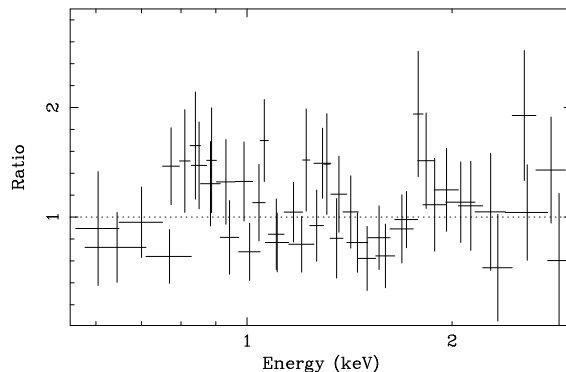


Figure 2. The ratio of the SIS data and a power-law model with $\Gamma = 2$. Possible emission features are seen at 0.87, 1.32, and 1.86 keV.

component with a column density over 10^{24} cm^{-2} , similar to Circinus Galaxy (Matt et al 1999), NGC6240 (Vignati et al 1999) and NGC4945 (Iwasawa et al 1993; Done et al 1996; Guainazzi et al 2000; Madejski et al 2000). In the soft X-ray band, marginal evidence for emission-line features are found below 3 keV in the ASCA SIS spectrum, which require reflection from partially ionized gas. Details of the spectral components mentioned above are given in the following sections.

4.2 The ASCA data

As Fig. 1 shows, the 0.6–3 keV spectrum can be described roughly with a power-law of $\Gamma \sim 2$. Although a simple power-law fit provides a reasonably good fit ($\chi^2 = 64.0$ for 68 degrees of freedom with $\Gamma = 2.1 \pm 0.3$) to the SIS data, possible line-like features can also be seen (Fig. 2). Only a feature at 0.87 ± 0.04 keV is detected with over 90 per cent significance according to the F-test when a narrow gaussian is fitted, while the other two features at 1.32 ± 0.06 and 1.86 ± 0.16 keV are less significant. The equivalent widths of these line features range between 80–140 eV. The 0.87 keV feature can be due to a OVIII recombination continuum (see Griffiths et al 1998 for a similar feature in the ASCA spectrum of Mrk 3 where they inferred $\xi \sim 500$ for the reflecting matter) or part of the Fe-L blend (e.g., FeXVII). The features at 1.32 and 1.86 keV are consistent with recombination lines from MgXI(1.34 keV) and SiXIII(1.85 keV), respectively. These features in the soft X-ray band could also originate from thermal emission from a starburst. However, the optical and infrared properties of this object suggest that starburst activity is weak even if it is present.

The Fe K line is found at a rest-energy of 6.37 ± 0.03 keV. No significant broadening is found (the 90 per cent upper limit is 110 eV in the gaussian dispersion, σ). The line flux is $2.1^{+0.5}_{-0.4} \times 10^{-5}$ ph s $^{-1}$ cm $^{-2}$, and the corresponding equivalent width is $\simeq 1.1$ keV with respect to the neighbouring flat continuum.

As mentioned in the previous section, the ASCA spectrum can be described with a sum of reflections from cold and ionized matter (also see Matt et al 2000). The Fe K band spectrum is well explained by reflection from thick, cold matter. The hard continuum fits well the reflection spectrum of `pexrav`. The soft X-ray emission-line features could originate from photoionized gas which also reflects a small fraction of the continuum light of the hidden central source. In this case, the photoionized gas should be optically thin, and the ionization parameter ξ is a few hundreds.

Reflection from mildly ionized, optically thick matter is a possible alternative to explain the whole ASCA band spectrum, as proposed for the Circinus Galaxy (Bianchi et al 2001). Note that the Fe K line remains at 6.4 keV and some excess soft X-ray emission is produced when $\xi \leq 30$. However, this possibility does not appear to be the case in Tol 0109–383. We have compared the $\xi = 30$ reflection spectrum of Ross, Fabian & Young (1999) with the data. The data above 3 keV are too hard to match the model spectrum, indicating that the Fe K band emission is produced in matter significantly less ionized than $\xi = 30$. Therefore a combination of reflection both from cold and highly ionized gas is more likely.

4.3 The BeppoSAX data

The data obtained from the LECS and MECS are in good agreement with the ASCA data below the Fe K band. The MECS data show a higher centroid-energy of 6.63 ± 0.09 keV with significant broadening ($\sigma = 0.22^{+0.11}_{-0.12}$ keV) for the Fe K line. A slightly higher line intensity of $2.6^{+1.0}_{-0.8} \times 10^{-5}$ ph s $^{-1}$ cm $^{-2}$ is also obtained. A likely cause of the line broadening would be a blend of a 6.4 keV line and a higher ionization line, e.g., FeXXV (6.7 keV), which should be resolved with the ASCA SIS, owing to the higher spectral resolution than the MECS and the GIS. However, no evidence for a higher energy lines is found in the ASCA data. This could be due to the gain shift problem with the MECS, although the offset is larger than that usually found (see e.g., Dupke & Arnaud 2001). Another possible reason for this is the spectral resolution which is not suitable for a complicated spectrum with a sharp drop on the higher energy side of the line due to the Fe K absorption edge. This could shift the line centroid to higher energy in a low resolution detector. A spectral analysis of the data from the ASCA GIS only, which is a similar detector to the MECS, gives the line energy of $6.44^{+0.37}_{-0.10}$ keV. The large error for the GIS line energy towards higher energies is suggestive but not conclusive enough to settle the problem. Since a narrow line at 6.4 keV is more plausible on the physical ground given the continuum shape, and an unexpected gain drift in the detector could lead to the line broadening, we are cautious about an immediate interpretation of the discrepancy.

The excess hard X-ray emission seen in the PDS data is most probably due to a strongly absorbed primary source. The 7–10 keV MECS flux is marginally lower (by ~ 30 per

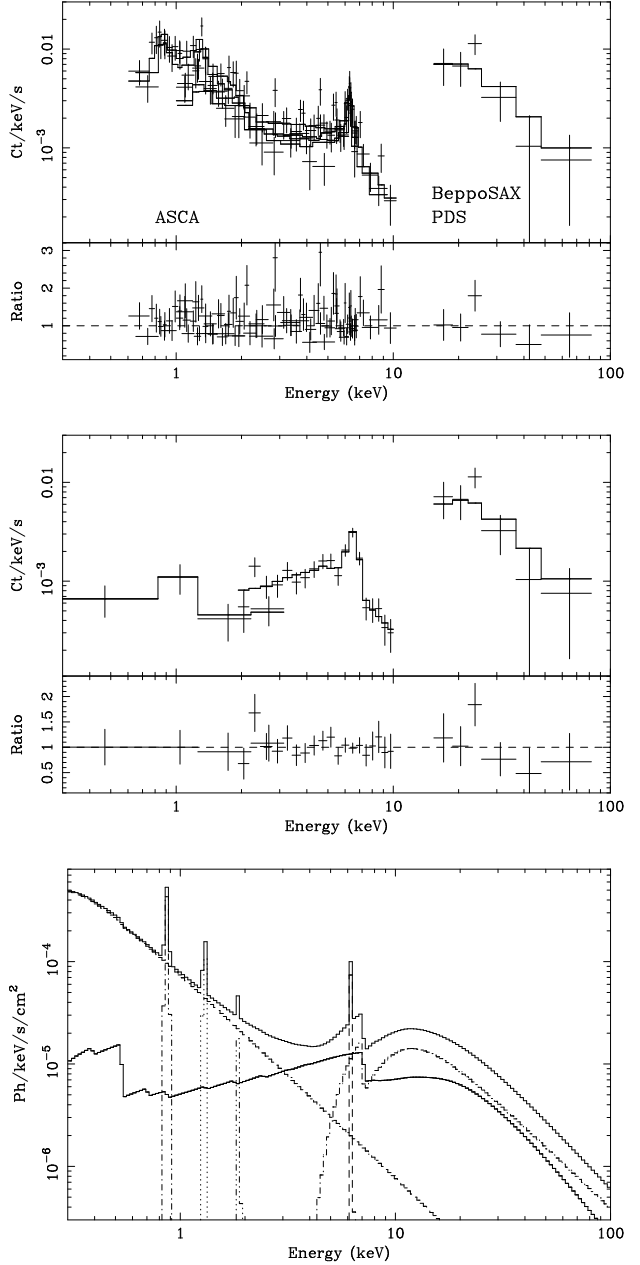


Figure 3. Upper panel: the ASCA data from the four detectors and the BeppoSAX PDS data of Tol 0109–383, fitted by the model consisting of cold and warm reflection and a strongly absorbed power-law. Gaussian lines at the rest-energies of 0.87, 1.34, 1.86 and 6.4 keV are also included. Middle panel: The BeppoSAX LECS, MECS and PDS data of Tol 0109–383, fitted with the same model as above apart from the absorption column density and iron K line parameters (see text). Lower panel: The best-fit model for the ASCA+PDS data, consisting of components given Table 2.

cent) than that measured by ASCA, which could be attributed to an intrinsic change in the low energy tail of the absorbed component. Spectral fits to the ASCA data (with the BeppoSAX PDS data) and the BeppoSAX data are presented in Fig. 3. Apart from the Fe K line and absorption column density, the fitted models are identical. The unabsorbed source is assumed to have a power-law spectrum with

Table 2. The spectral fits to the ASCA and BeppoSAX data of Tol 0109–383. In fitting, free parameters are normalizations of respective components, the absorption column density, and the Fe K line parameters. The line energies of the three soft X-ray lines are fixed. While the line fluxes are left as free parameters in the fit of the ASCA data, they are fixed at the ASCA values for the fit to the BeppoSAX data. All the spectral components are modified by Galactic absorption of $N_{\text{H}} = 1.8 \times 10^{20} \text{cm}^{-2}$. The line width of the Fe K line is measured by gaussian dispersion in keV.

Spectral components	Model				
Soft X-ray emission	Power-law ($\Gamma = 2.0$)				
	3 narrow gaussian lines (at 0.87, 1.36 and 1.86 keV)				
Cold reflection	PEXRAV ($\Gamma = 2.0$, reflection only)				
	A gaussian line (Fe K); see the separate table				
Absorbed central source	Power-law ($\Gamma = 2.0$)				
	Cold absorption: $N_{\text{H}} = 1.6_{-1.0}^{+1.0} \times 10^{24} \text{cm}^{-2}$ (ASCA+PDS)				
	$N_{\text{H}} = 3.5_{-1.4}^{+1.8} \times 10^{24} \text{cm}^{-2}$ (SAX)				
Fe K line Measurements	Energy (keV)	Line width (keV)	Line flux $\text{ph s}^{-1} \text{cm}^{-2}$	Quality of fit	χ^2 / dof
ASCA	6.37 ± 0.03	< 0.11	$2.1_{-0.4}^{+0.5} \times 10^{-5}$	ASCA+PDS	187.3 / 186
BeppoSAX	6.63 ± 0.09	$0.22_{-0.12}^{+0.11}$	$2.6_{-0.8}^{+1.0} \times 10^{-5}$	BeppoSAX	16.1 / 18

Table 3. High excitation lines and infrared colours of Compton-thick Seyfert 2 galaxies. Optical Seyfert type is given in the second column. PBLR represents a Seyfert 2 galaxy with Polarized Broad-Line Region. The values of $[\text{FeVII}]\lambda 6087/[\text{OIII}]\lambda 5007$ have not been corrected for internal reddening. S_{60}/S_{25} and S_{25}/S_{12} are the ratio of IRAS flux densities at 60 and 25 μm , and 25 and 12 μm . $R(L, 25)$ is the mid-infrared diagnostic of a dusty torus introduced by Murayama et al (2000), as defined by $R(L, 25) = \log[(\nu_{3.5\mu\text{m}} S_{\nu 3.5})/(\nu_{25\mu\text{m}} S_{\nu 25})]$. References: $<[\text{FeVII}]/[\text{OIII}]>$ 1: Murayama et al 1998; 2: Nagao et al 2000; 3: Alloin et al 1992; 4: Kleinmann et al 1988; 5: Tran et al 2000; $<\text{IRAS flux}>$ 6: IRAS Faint Source Catalogue; 7: IRAS Team 1983; $<\text{L-band photometry}>$ 4: Kleinmann et al 1988; 8: Glass & Moorwood 1985; 9: Murayama et al 2000. † Contamination from the host galaxy is likely. ‡ The L band photometry is approximated by the L' data.

Galaxy name	Class	$[\text{FeVII}]/[\text{OIII}]$	S_{60}/S_{25}	$R(L, 25)$	Ref.
Tol 0109–383	PBLR	5.36×10^{-2}	1.03	−0.036	1,6,8
NGC 1068	PBLR	1.87×10^{-2}	2.07	−0.79	2,6,9
NGC 7674	PBLR	1.59×10^{-2}	2.94	−0.76†	2,6,9
IRAS 09104+4109	PBLR	1.95×10^{-2}	1.57	−1.25‡	4,5,6
Circinus galaxy	S2	1.69×10^{-2}	4.31	−1.16†	2,7,9
NGC 5643	S2	—	5.34	−1.26	2,6,8
ESO 138-G1	S2	2.71×10^{-2}	—	—	3
Mrk 231	S1	—	3.69	−0.53	6,9

$\Gamma = 2$ and no high energy cut-off. We utilized `pexrav` and a gaussian Fe K line to model the cold reflection. The reflecting slab is assumed to be of Solar abundance and nearly face-on ($\sim 20^\circ$ in inclination). The soft X-ray continuum is described by a $\Gamma = 2$ power-law modified only by Galactic absorption. The X-ray absorption column density to the central source is estimated to be $(1.6 \pm 1.0) \times 10^{24} \text{cm}^{-2}$ from the ASCA+PDS and $3.5_{-1.4}^{+1.8} \times 10^{24} \text{cm}^{-2}$ from the three detectors of BeppoSAX. Since the ASCA and BeppoSAX observations are not simultaneous, the slightly smaller N_{H} value obtained from the ASCA+PDS fit might suggest a luminosity increase of the central source, assuming that the column density is not variable. The three continuum components plus the gaussian lines described above (and in Table 2) fit the data well ($\chi^2 = 187.3$ for 186 degrees of freedom for ASCA+PDS; $\chi^2 = 16.1$ for 18 degrees of freedom for LECS+MECS+PDS), as shown in Fig. 3. Although the data do not provide a good constraint on the continuum slope if it is left as a free parameter, a flat continuum with a photon-index smaller than 1.5 can be ruled out. The effect of Compton scattering in this large absorbing column

(e.g., Matt, Pompilio & La Franca 1999) is not taken into account here. An appropriate correction will be applied on estimating the absorption-corrected luminosity.

The observed 0.5–2 keV, 2–10 keV, and 20–100 keV fluxes are $2.2 \times 10^{-13} \text{erg cm}^{-2} \text{s}^{-1}$, $1.6 \times 10^{-12} \text{erg cm}^{-2} \text{s}^{-1}$ and $1.8 \times 10^{-11} \text{erg cm}^{-2} \text{s}^{-1}$, respectively.

5 DISCUSSION

The ASCA spectrum is consistent with a reflection-dominated emission, as concluded by Collinge & Brandt (2000). The BeppoSAX PDS detection of a transmitted component at higher energies allows us to measure the column density of the Thomson-thick absorber ($N_{\text{H}} \sim 2\text{--}3 \times 10^{24} \text{cm}^{-2}$, or Thomson depth $\tau_{\text{T}} \sim 2$, assuming Solar abundance). The best estimate of the absorption-corrected 2–10 keV luminosity of the central source is $7 \times 10^{42} \gamma \text{erg s}^{-1}$ for our assumed source distance. With the flattest limit of the spectral slope of the central source, $\Gamma = 1.5$, this value is a factor of 2 larger. Note that the correction for Compton-scattering (Matt et al 1999) has been made ($\gamma = 1$ for a

spherical obscuration; the value increases to ~ 3 if the covering fraction is small for $N_{\text{H}} = 3 \times 10^{24} \text{cm}^{-2}$).

The reflected fraction (i.e., the luminosity ratio of the observed and the absorption-corrected continuum) in the 2–10 keV band, where most of the observed flux comes from cold reflection, is $\sim 5\gamma^{-1}$ per cent. Compared with the albedo from cold matter, this means that a quarter to half of the reflection expected from a slab subtending at 2π is visible to us. If the cold reflection occurs at the inner surface of the obscuring torus, then a large fraction of the surface is exposed to our view.

The optical polarization of the nucleus of Tol 0109–383 is relatively high (1.5 per cent, Brindle et al 1990; 2.3 per cent, Moran et al 2000 in the V band) and polarized broad emission lines have been detected (Moran et al 2000). Note that broad Balmer emission has been detected even in the direct light in Tol 0109–383 (Murayama et al 1998). Several authors have argued that a moderately inclined obscuring torus is preferred for detecting PBLR (e.g., Heisler et al 1997; Taniguchi & Anabuki 1999). The PBLR Seyfert 2 sample of Heisler et al (1997) tends to have warm IRAS colours, which is naturally explained by the viewing angle effect, i.e., hot dust at inner radii is more visible in a more inclined system (e.g., Pier & Krolik 1992). We have verified that this trend holds for the distance-limited spectropolarimetric survey sample of Moran et al (2000). Awaki et al (2000), however, prefer a large size of the scattering regions to the viewing angle effect for detectability of the PBLR.

For Tol 0109–383, the viewing angle appears to be an important key. Observed properties listed below all point to us looking into the inner part of the active nucleus: 1) the relatively large X-ray reflection fraction from cold matter, as discussed above; 2) the detection of broad Balmer emission and permitted FeII emission in direct light (Murayama et al 1998); 3) the very warm IRAS colour (see Table 3); and 4) the presence of high-ionization emission lines, particularly the high [FeVII] λ 6078/[OIII] λ 5007 ratio (see Table 3).

As mentioned in the Introduction, some high ionization emission lines may originate in the inner surface of the optically thick torus (e.g., Pier & Voit 1995; Murayama & Taniguchi 1998), thus could be an indicator of the torus viewing angle. Nagao et al (2000) have shown that the [FeVII]/[OIII] ratio is markedly different between the two types of Seyferts. A good segregation is also seen with the mid-infrared flux ratio of $3.5\mu\text{m}$ (*L* band) and $25\mu\text{m}$ (Murayama, Mouri & Taniguchi 2000). The IRAS S_{60}/S_{25} ratio may not necessarily be a good indicator of torus orientation (Fadda et al 1998; Murayama, Mouri & Taniguchi 2000; Alexander 2001) since there must be a significant contribution to the $60\mu\text{m}$ flux from the host galaxy, although Heisler et al (1997) show that the PBLR and non-PBLR Seyfert-2 galaxies are well separated using this ratio. Based on the compact dusty torus model by Pier & Krolik (1992), Murayama et al (2000) demonstrate that the flux ratio of *L*-band and $25\mu\text{m}$ is a good diagnostic to the torus orientation, provided contamination from starburst (or a host galaxy) is negligible.

We show the values of possible orientation measures mentioned above ([FeVII]/[OIII] ratio, S_{60}/S_{25} and $R(L, 25) = \log[(\nu_{3.5\mu\text{m}} S_{\nu 3.5})/(\nu_{25\mu\text{m}} S_{\nu 25})]$) of Tol 0109–383 along with other Compton-thick Seyfert galaxies (Collinge & Brandt 2000; Matt et al 1997; Matt et al 1999; Risaliti et al 1999; Malaguti et al 1999; Iwasawa et al 2000;

Maloney & Reynolds 2000), some of which have been known as PBLR Seyfert 2s, in Table 3. Two other Compton-thick sources, NGC4945 and NGC6240, are not included, since a starburst dominates the optical to mid-infrared wave bands in those galaxies. The high [FeVII]/[OIII] ratio and the flat infrared spectrum, implied from the small S_{60}/S_{25} and large $R(L, 25)$ of Tol 0109–383 are consistent with a picture that the interior of the torus is largely exposed, compared to the other Compton-thick Seyfert 2s. The lack of correlation between the X-ray absorption column density (Bassani et al 1999) and the [FeVII]/[OIII] ratio (Nagao et al 2000) probably means that the structure of obscuring torii in Seyfert 2 galaxies is not unique.

Despite the close resemblance to a Seyfert 1 nucleus, the central X-ray source in Tol 0109–383 is hidden behind heavy obscuration. The large column of absorbing gas is unlikely to be associated with the dust lanes imaged by the HST (Malkan et al 1998). This is clearly a geometrical effect and the X-ray absorption is likely to occur on small radii, perhaps on the parsec scale, as originally proposed by Krolik & Begelman (1988) and also by Matt (2000). More exposure of an optical Seyfert 1 nucleus is found in Mrk 231, for which an X-ray nucleus hidden by a Compton-thick absorber has been suggested by Maloney & Reynolds (2000). The location of very thick X-ray absorbing matter may be distinct from the torus hiding the BLR (or an optical nucleus in Seyfert 2 galaxies), and could be in a special form (e.g., Elvis 2000).

ACKNOWLEDGEMENTS

We thank the BeppoSAX and ASCA teams for their efforts on operation of the satellites, and the calibration and maintenance of the software. ACF and KI thank the Royal Society and PPARC for support, respectively.

REFERENCES

- Alexander D.M., 2001, MNRAS, 320, L15
 Alloin D., Bica, E., Bonatto C., Prugniel P., 1992, A&A, 266, 117
 Antonucci R.R.J., 1993, ARAA, 31, 473
 ASCA Guest Observer Facility (GOF), 1999, <http://heasarc.gsfc.nasa.gov/docs/asca/watchout.html>
 Awaki H., Ueno S., Taniguchi Y., Weaver K.A., 2000, ApJ, 542, 175
 Bassani L., Dadina M., Maiolino R., Salvati M., Risaliti G., Della Cecca R., Matt G., Zamorani G., 1999, ApJS, 121, 473
 Bianchi S., Matt G., Iwasawa K., 2001, MNRAS, 322, 669
 Boella G., Butler R.C., Perola G.C., Piro L., Scarsi L., Bleeker J.A.M., 1997a, A&AS, 122, 299
 Boella G., et al, 1997b, A&AS, 122, 327
 Boisson C., Durret F., 1986, A&A, 168, 32
 Brindle C., Hough J.H., Bailey J.A., Axon D.J., Ward M.J., Sparks W.B., McLean I.S., 1990, MNRAS, 244, 577
 Collinge M.J., Brandt W.N., 2000, MNRAS, 317, L35
 Da Costa L.N., Pellegrini P.S., Davis M., Meiksin A., Sargent W.L.W., Tonry J.L., 1991, ApJS, 75, 935
 De Robertis M.M., Osterbrock D.E., 1986, ApJ, 301, 727
 de Vaucouleurs G., et al, 1991, Third Reference Catalogue of Bright Galaxies (New York: Springer)
 Dickey J.M., Lockman F.J., 1990, ARAA, 28, 215
 Done C., Madejski G.M., Smith D.A., 1996, ApJ, 463, L63
 Durret F., Bergeron J., 1988, A&A, 173, 219
 Elvis M., 2000, ApJ, 545, 63

- Fadda D., Giuricin G., Granato G., Vecchies D., 1998, *ApJ*, 96, 117
- Fosbury R.A.E., Sansom A.E., 1985, *MNRAS*, 204, 1231
- Frontera F., Costa R., dal Fiume D., Feroci M., Nicastro L., Orlandini M., Palazzi E., Zavattini G., 1997, *Proc. SPIE*, 3114, 206
- Ghisellini G., Matt G., Haardt F., 1994, *MNRAS*, 267, 743
- Glass I.S., Moorwood A.F.M., 1985, *MNRAS*, 214, 429
- Goodrich R.W., Veilleux S., Hill G.J., 1994, *ApJ*, 422, 521
- Green P.J., Anderson S.F., Ward M.J., 1992, *MNRAS*, 254, 30
- Griffiths R.G., Warwick R.S., Georgantopoulos I., Done C., Smith D.A., 1998, *MNRAS*, 298, 1159
- Guainazzi M., Matt G., Brandt W.N., Antonelli L.A., Barr P., Bassani L., 2000, *A&A*, 356, 463
- Heckman T.M., 1995, *ApJ*, 446, 101
- Heisler C.A., Lumsden S.L., Bailey J.A., 1997, *Nat*, 385, 700
- IRAS Team, 1983, *Nat*, 303, 480
- Iwasawa K., Koyama K., Awaki H., Kunieda H., Makishima K., Tsuru T., Ohashi T., Nakai N., 1993, *ApJ*, 409, 155
- Iwasawa K., Fabian A.C., Etori S., 2000, *MNRAS*, 321, L15
- Kleinmann S.G., Hamilton D., Keel W.C., Wynn-Williams C.G., Eaeles S.A., Becklin E.E., Kuntz K.D., 1988, *ApJ*, 328, 161
- Krolik J.H., Begelman M.C., 1988, *ApJ*, 329, 702
- Madejski G., Zycki P., Done C., Valinia A., Blanco P., Rothschild R., Turek B., 2000, *ApJ*, 535, L87
- Magdziarz P., Zdziarski A., 1995, *MNRAS*, 273, 837
- Maiolino R., Salvati M., Bassani L., Dadina M., Della Cecca R., Matt G., Risaliti G., Zamorani G., 1998, *A&A*, 338, 781
- Malaguti G., et al, 1998, *A&A*, 331, 519
- Malkan M.A., Gorjian V., Tam R., 1998, *ApJS*, 117, 25
- Maloney P.R., Reynolds C.S., 2000, *ApJ*, 545, L23
- Matt G., et al, 1997, *A&A*, 325, L13
- Matt G., Pompilio F., La Franca F., 1999, *New Astronomy*, 4, 191
- Matt G., et al, 1999, *A&A*, 341, L39
- Matt G., Fabian A.C., Guainazzi M., Iwasawa K., Bassani L., Malaguti G., 2000, *MNRAS*, 318, 173
- Matt G., 2000, *A&A*, 355, L31
- Moran E.C., Barth A.J., Kay L.E., Filippenko A.V., 2000, *ApJ*, 540, L73
- Morganti R., Tsvetanov Z.I., Gallimore J., Allen M.G., 1999, *A&AS*, 137, 457
- Mulchaey J.S., Koratkar A., Ward M.J., Wilson A.S., Whittle M., Antonucci R.R.J., Kinney A.L., Hurt T., 1994, *ApJ*, 436, 586
- Murayama T., Taniguchi Y., Iwasawa K., 1998, *AJ*, 115, 460
- Murayama T., Taniguchi Y., 1998, *ApJ*, 497, L9
- Murayama T., Mouri H., Taniguchi Y., 2000, *ApJ*, 528, 179
- Nagao T., Taniguchi Y., Murayama T., 2000, *AJ*, 119, 2605
- Parmar A.N., 1997, *A&AS*, 122, 309
- Pier E., Krolik J., 1992, *ApJ*, 401, 99
- Pier E.A., Voit M.G., 1995, *ApJ*, 450, 628
- Risaliti G., Maiolino R., Salvati M., 1999, *ApJ*, 522, 157
- Ross R.R., Fabian A.C., Young A.J., 1999, *MNRAS*, 306, 461
- Rush B., Malkan M.A., Fink H.H., Voges W., 1996, *ApJ*, 471, 190
- Tanaka Y., Inoue H., Holt S., 1994, *PASJ*, 46, L37
- Taniguchi Y., Anabuki N., 1999, *ApJ*, 521, L103
- Taniguchi Y., Murayama T., 1998, *ApJ*, 501, L25
- Threan A., Pedlar A., Kukula M.J., Baum S.A., O’Dea C.P., 2000, *MNRAS*, 314, 573
- Tran H.D., Cohen M.H., Villar-Martin M., 2000, *AJ*, 120, 562
- Ulvestad J.S., Wilson A.S., 1989, *ApJ*, 343, 659
- Vignati P., et al, 1999, *A&A*, 349, L57
- Voges W., et al, 1999, *A&A*, 349, 389